Controlled Undercooling of Liquid Iron In Contact with Al_2O_3 Substrates under Varying Oxygen Partial Pressures

MARTIN E. VALDEZ, PELLO URANGA, KATSUHIRO FUCHIGAMI, H. SHIBATA, and ALAN W. CRAMB

The objective of this study was to determine the conditions under which alumina can act as a heterogeneous nucleant to initiate the solidification of undercooled liquid iron. The undercooling of a pure iron sessile droplet in contact with Al_2O_3 substrates was measured under controlled oxygen partial pressures by observing droplet recalescence. The experimental results indicated that the undercooling of liquid iron, in contact with an Al_2O_3 substrate, did not have a unique value, varied from 0 °C to 290 °C, and was significantly affected by the oxygen content of the gas phase and the degree of interaction between the oxide and the metal. Deep undercoolings are possible at low oxygen potentials, provided the oxygen potential is such that substantial substrate decomposition does not occur. The measured undercooling was a strong function of gas phase oxygen content and a maximum in undercooling of 290 °C was measured at $PO_2 = 10^{-19}$ atm. The variation in undercooling was related to the wetting of the substrate by the liquid metal, where the deepest undercoolings occurred when the highest contact angle between the substrate and the liquid droplet was achieved.

I. INTRODUCTION

THE presence of nonmetallic inclusions in steel is associated with low productivity and the generation of defects in the downstream process and, as a result, low-quality products. The field that studies the minimization of the effect of inclusions on the steelmaking process and on the final product properties is usual called ''clean steel.'' By the end of the last century, several researchers proposed methods to make use of inclusions in a beneficial way. This new concept was called ''oxide metallurgy,''[1] and it highlights the possibility of a beneficial use of existing inclusions to control metallurgical changes. In the continuous casting process, since the structure of a solid depends strongly upon the initial solidification condition, and this initial solidification condition in turn depends upon the type and density of nucleants, the inclusions in the steel can be designed to maximize their effect as inoculants.

The general objective of the use of oxide metallurgy in casting is to address the importance of nonmetallic inclusions in the definition of the solidification structure and to determine the conditions for its application in the production of bulk steel. The objective of this work is to determine the fundamental conditions under which the inclusions present in liquid steel can act as heterogeneous nucleants for solidification.

MARTIN E. VALDEZ, Graduate Student and Postdoctoral Fellow, formerly with the Department of Materials Science and Engineering, Carnegie Mellon University, is with Tenaris/CINI, Campana, Argentina B2804MHA. Contact e-mail: martinvaldez@alumni.cmu.edu PELLO URANGA, Researcher, is with CEIT and TECNUN (University of Navarra), E-20018 Donostia-San Sebastian, Basque Country, Spain. KATSUHIRO FUCHIGAMI, Researcher, is with the Research and Development Lab., Nippon Steel Corporation at Oita, Oita, Japan 870-0992. H. SHIBATA, Lecturer, is with the Institute of Multidisciplinary Research for Advanced Materials, Tohoku University, Sendai, Japan 980-8577. ALAN W. CRAMB, formerly with the Department of Materials Science and Engineering, Carnegie Mellon University, Pittsburgh, PA 15213, is Dean of Engineering, Rensselaer Polytechnic Institute, Troy, NY 12180.

Manuscript submitted February 11, 2006.

There are a limited number of articles in the literature that discuss the importance of inclusions on the determination of the solidification structure of metals. Most of these articles came from the field of welding[2,3,4] but there are some references to the production of steel with 100 pct equiaxed structure in Posco[5] and Sumitomo.[6] There are also some interesting insights into the mechanisms of heterogeneous nucleation from the external inoculation process that has been long used in the production of aluminum.[7,8]

By reviewing the effect of inclusions on the solidification of the welding process, aluminum production, and the attempts of the steel industry, it is possible to list some factors that are important for solidification control through the use of inclusions in the casting process. From the analysis of weld pool solidification, it is well reported that the amount of equiaxed zone depends on the type of inclusions or inoculant particles and that the lattice disregistry between inclusions and solid metal may define undercooling.[2,3,4] In Al-alloy casting,[7,8] a fine, uniform, and equiaxed microstructure can be achieved by inoculation, but because the inoculants are potent and the nucleation undercooling is very low, the classical spherical-cap model is not useful in explaining the results. Alternative models have shown that the adsorption of solutes in the substrate/melt interface as well as the reaction between the substrates and the melt can have effects on solidification that are not expected from the classical nucleation theory.

The design of a process in which the undercooling, and hence the solidification structure, can be controlled requires a deep understanding of the factors that define when and where nucleation occurs. The objective of this article is to determine the effect of oxygen partial pressure on the undercooling of iron in contact with alumina. Particular attention was paid to determining the oxygen partial pressure in the gas phase, as it is well known that varying oxygen partial pressure in the gas phase in an equilibrium experiment varies the interfacial properties of both the liquid in contact with the gas and the liquid in contact with the substrate.

II. UNDERCOOLING MEASUREMENTS

The accurate measurement of undercooling in a homogeneous nucleation situation requires the elimination of available nucleation surfaces during measurement. On the other hand, the accurate measurement of undercooling in a heterogeneous-nucleation situation requires the control of the surfaces available for nucleation. Table I shows undercooling measurements for Fe alloys using different techniques.

If a liquid metal is divided into small droplets, the impurities responsible for heterogeneous nucleation are isolated and some droplets may remain free of impurities. Using this concept, Turnbull and co-workers[11] pioneered a technique for measuring homogeneous nucleation by measuring the maximum undercooling of a large number of small droplets. The maximum undercooling measured for iron under these conditions was 295 °C.

The presence of a container always has an effect,[16] unless there is no direct contact with the container, such as in levitation[17–20] or encasement.[21] In encasing techniques, the metal is isolated from the crucible by a viscous slag. Undercoolings as high as 300 °C were obtained for Fe alloys by Umeda[9] and Kattamis.[10] On the contrary, there are experiments in which the crucible is always present, but the effect of ''particles'' can also be measured provided their power as heterogeneous nucleation agents is stronger that the crucible itself. Rastogi[14] and Kudoh[12,13] measured the undercooling of steels with different inclusions in Al_2O_3 crucibles. Mizoguchi[22] measured the undercooling of pure iron and Fe-Ni alloys containing TiN, Al_2O_3, and Ti_2O_3 particles using a differential scanning calorimetry (DSC). Mizoguchi's experiments were performed in Al_2O_3 crucibles and under ultra-high-purity Ar gas atmosphere at a heating rate of 20 °C/min and cooling rates from 5 °C/min to 70 °C/min. In these experiments, the difference between the melting point during heating and the starting point of nucleation during cooling was defined as the undercooling for the heterogeneous nucleation. The maximum undercooling of 164 °C was achieved for pure iron samples.

III. EXPERIMENTAL AND MATERIALS

The experimental approach of this work consisted of measuring the undercooling of a pure iron droplet on top of oxide substrates, using a sessile drop technique setup. The sessile drop technique is usually used to measure the contact angle and surface tension of liquid metals. The undercooling was measured by slowly cooling the droplet/substrate system and by detecting solidification due to the increase in brightness of the droplet when the latent heat was released. Figure 1 shows the change in brightness as detected by the CCD camera.

A. *Experimental Procedure and Apparatus*

The setup used for the measurement of undercooling is similar to the one used for contact angle measurement. Figure 2 shows a schematic of the experimental apparatus.

The furnace used was a Lindberg $MoSi_2$ resistance furnace. The chamber of the furnace is an alumina tube of high quality that allows for gas composition control without air infiltration. The alumina tubes were provided by Vesuvius Mc Danel, (Beaver Falls, PA) and were made of cast alumina 99.8 pct purity (1000-mm length, 3-in. o.d., and 2.75-in. i.d.). The heating was controlled by a thermocouple placed outside the main chamber. The difference between the setup temperature of the furnace in Figure 2 and the center of the furnace where the sample is located was 55 °C. A piece of pure iron (purity 99.995 pct) of approximately 0.25 g was placed inside the furnace on top of an Al_2O_3 substrate (A-plane single crystals from Alfa Aesar, Ward Hill, MA, or polycrystalline substrates from Vesuvius). The system was closed and different gases (Ar, Ar-5 pct H_2, or CO-CO_2 mixture) were flown inside the furnace with the objective of purging the system and controlling the oxygen partial

Table I. Undercooling Measurements for Fe Alloys

Author	Reference	Material	Method		ΔT*
Flemings	9	316 stainless	emulsion in glass		475
Kattamis	10	Fe – 25 pct Ni	encasing in glass or slag		300
Turnbull	11	Fe	small droplets on quartz or Pyrex		295
Kudoh	12	Fe-C	in crucible		284
Umeda	9	Fe-C alloys	encasing in slag		280
Kudoh	13	carbon steel	in crucible		232
				no inclusions	127
				no inclusions	112
				Al_2O_3 inclusions	96
Rastogi	14	Fe	in Al_2O_3 crucible	Al_2O_3 inclusions	88
				$xCaO{\cdot}yAl_2O_3$ inclusions	187
				Ti_xO_y inclusions	41
				Al_2O_3 + TiN inclusions	151
		Fe		no inclusions	164
		Fe	DTA	Ti_2O_3 inclusions	57
Mizoguchi	15	Fe-0 to 6 pct Ni	Al_2O_3 crucible	TiN inclusions	13
		Fe-6 to 29 pct Ni			68
		Fe-0 to 9 pct Ni		Al_2O_3 inclusions	36 to 40

*Maximum ΔT observed.

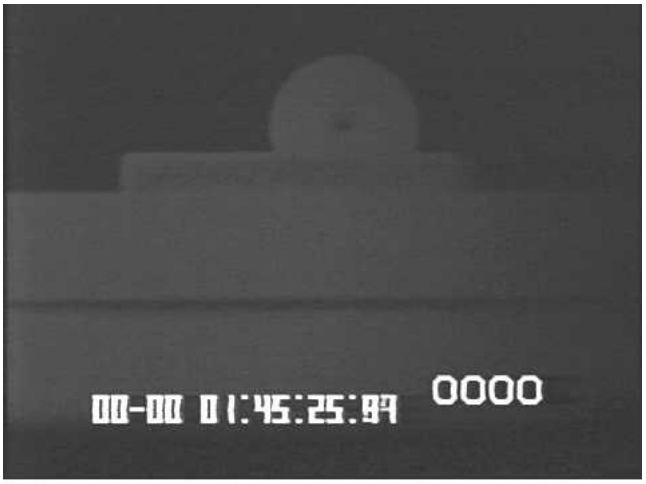

Before Recalesence
1h 45 min. 25 sec. 91 centiseconds

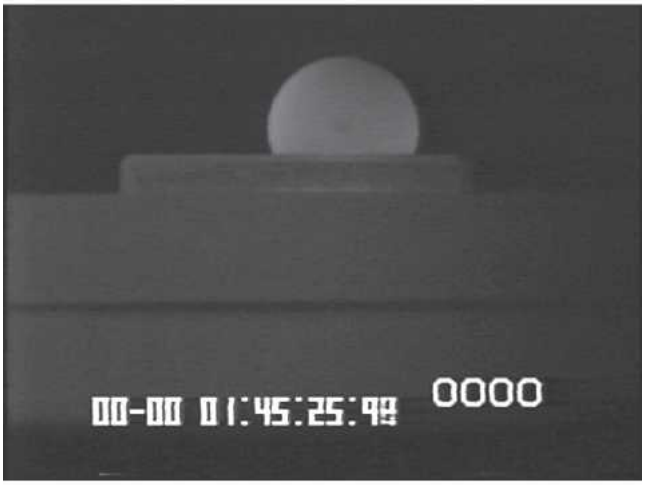

After Recalesence
1h 45 min. 25 sec. 98 centiseconds

Fig. 1—Photograph of the droplet before and after recalescense showing that the start of solidification is detected as a sudden change in brightness.

pressure. The flow rate was set up between 100 and 200 mL/min, and a time period of approximately 5 hours was necessary to purge the entire system from any trace of air. Downstream from the furnace, the gas was flown through an oxygen sensor at 800 °C (solid-stabilized zirconia from Australian Oxytrol Systems, Eaglehawk, Victoria, Australia) that continuously monitored the oxygen partial pressure (PO_2) in the gas. Two oxygen sensors (one in the entrance, ''IN,'' and another one in the exit, ''OUT'') were used in special cases and for calibration purposes.

The sample was heated at 3 °C/min to the soaking temperature and left at this temperature for 1 hour before cooling. The soaking temperature was 1600 °C. The cooling rate was also 3 °C/min. Slow cooling rates were necessary to avoid any inertia on the temperature as well as to assure a constant temperature in the sample and that the system was not controlled by heat transfer. The recording of the video (Sony CCD-IRIS color video camera model DXC-107A) started at the same time as the cooling. Further analysis of the video allowed the determination of the contact angle of the system at 1600 °C, the degree of undercooling necessary for solidification, the rate of movement of the solidification front, and the place of initiation of solidification.

The idea behind these experiments was to determine which oxides promote the solidification of iron by providing a suitable surface for nucleation and, on the contrary, which oxides and under which conditions the metal can be deeply undercooled. In order to understand the phenomena observed in more detail, the results were confirmed using a differential thermal analysis (DTA) apparatus. The DTA used for the experiments was a DSC 2910–DTA 1600 from TA Instruments (New Castle, DE). During the experiments, the temperature difference between the sample (pure iron) and the reference was continuously measured. The reference material used was alumina powder; the weight of iron used was 90 mg, and the weight of reference alumina powder was 59 mg. Since the alumina does not have any transformation at temperatures below 1600 °C, the transformations of the iron samples (solid state, melting, and solidification) can be detected as an increase or decrease in the temperature difference between both thermocouples.

B. *Oxygen Control*

A test chamber with a controlled/inert environment is one of the basic requirements for contact angle measurements.[23] This is because the oxygen content is known to affect the contact angle and surface tension of liquid metals[24–32] by affecting the surface energies involved in wetting (γ_{LG}, γ_{LO}, and γ_{OG}, where L = liquid, O = oxide substrate, and G = gas). Heterogeneous undercooling is also affected by the values of surface energies, but in the case of the liquid-solid-oxide system (γ_{LS}, γ_{LO}, and γ_{OS}), the control of the oxygen partial pressure (PO_2) is crucial. Different oxygen partial pressures were achieved by a combination of different gases (CO/CO_2 mixtures, Ar or Ar-5 pct H_2), by making the gas flow through different getters (Mg and Cu at 500 °C) and by placing titanium sponge in a furnace at 1000 °C on the path of the incoming gas and in a basket placed inside the main furnace. Table II shows the range of PO_2 that can be achieved with different experimental conditions.

The main causes of variation in the PO_2 are system leakage, the flow rate of the gas, and the type of flow inside the furnace. Leakage is more difficult to control as the PO_2 decreases, and can be caused, for example, by microcracking of the alumina tube due to tensions introduced by the thermal gradients. The gas flow rate has an influence on the reaction of the getters with the traces of oxygen in the gases. The type of flow has its effect on the transient time during which the incoming gas is modified. In general, the flow is a ''plug type'' in the incoming gas, while the out gas slowly changes its value due to the mixing in the furnace chamber. In general, the out gas is considered more representative of the gas composition inside the chamber. There is no straightforward way to calibrate the oxygen sensor for the measurements at very low oxygen potentials. In order to gather confidence in the measurements, the following issues were analyzed: (a) correction for electronic conductivity (it is not important for sensors working at 800 °C), (b) melting of aluminum (aluminum was kept liquid at 1600 °C

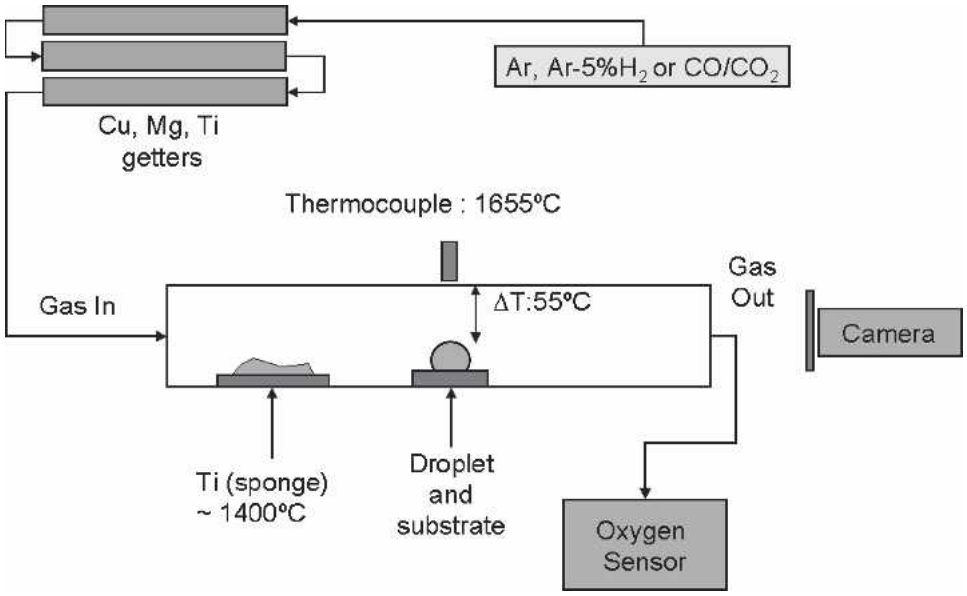

Fig. 2—Experimental apparatus showing the system to clean the gas upstream and an oxygen sensor downstream.

Table II. Experimental Conditions and the Corresponding Range of PO_2

Experimental Conditions			Range of PO_2
Ar	not gettered	—	$>10^{-8}$
CO/CO_2	—	—	10^{-13} to $10^{-9.5}$
Ar	Cu,Mg at 500 °C Ti at 1000 °C	Ti inside the furnace at 1400 °C	10^{-22} to 10^{-17}
Ar-5 pct H_2	Cu,Mg at 500 °C Ti at 1000 °C	Ti inside the furnace Ti at 1400 °C	10^{-23} to 10^{-21}

showing that the oxygen partial pressure was below the Al/Al_2O_3 equilibrium oxygen partial pressure of 1.11×10^{-20} at 1600 °C[33,34]), (c) the values of oxygen partial pressure were compared with the values measured by other authors,[24,31,35–40] (d) two oxygen sensors were placed in series and both measured the same PO_2, and (e) a minimum error in the PO_2 was measured using different gases as reference (*e.g.,* air *vs* gettered Ar *vs* nongettered Ar).

IV. RESULTS

A. *Undercooling and Contact Angle Measurement*

A first set of individual recalescense measurements (experiment 1) was done using polycrystalline alumina as a substrate using different gases. The main observation was that, in the case of Ar/H_2, the undercooling was around 50 °C, while in the case of Ar experiments, the undercooling was observed to be around 200 °C with a large scatter (160 °C to 260 °C).

In order to check the effect of the actual value of oxygen partial pressure, a series of undercooling experiments were performed using the same droplet but under different atmospheric conditions (experiment 2). Figure 3 shows the change in PO_2 and temperature of the furnace during the experiment (in this case, using pure Fe and polycrystalline Al_2O_3). The first part of the experiment was done under

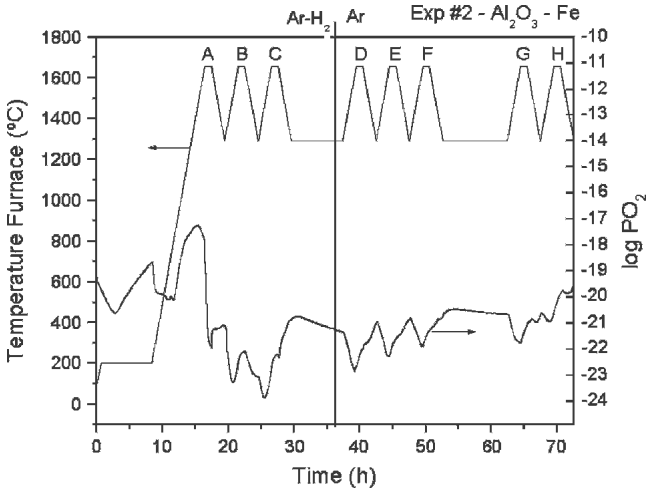

Fig. 3—Change in PO_2 and furnace setup temperature during experiment 2.

Ar/H_2, resulting in low oxygen partial pressure in the gas; the PO_2 decreases from 10^{-18} to 10^{-23} atm due to purging. After the gas was changed to Ar, the PO_2 slowly increases back to 10^{-20} atm. The variation in the oxygen partial pressure is, in general, due to the change in the availability of Cu, Mg, and Ti surfaces for oxidation. During multi-recalescense experiments, several sequenced experiments

were done without changing the getters to cause an increase in the PO_2.

The increase in PO_2 results on a change in the value of undercooling. The change in undercooling during experiment 2 is shown in Figure 4. The tendency is for the undercooling to increase as the PO_2 in the furnace increases. It is important to highlight that the change is significant, moving from above 75 °C in the experiments with low PO_2 to over 275 °C as the oxygen content in the gas increases. It is also important to emphasize that in the case of deep undercooling, due to the low cooling rates (3 °C/min), the sample remains undercooled for almost 90 minutes. Experiment 2A (Figure 4) shows that the increase in undercooling is not caused by the position in the sequence during the multirecalescense experiments but by the actual oxygen partial pressure. From the figure, it can also be observed that the difference in undercooling is not caused by the gas used but instead by the value of PO_2.

The maximum increase in undercooling should be limited by the homogeneous nucleation undercooling, suggested to be theoretically a value around 0.3 to 0.4 of the melting temperature[41] and measured experimentally by Turnbull for nucleation of small pure iron droplets[11] as 295 °C (Table I). It can also be limited by the hypercooled condition (280 °C to 320 °C).

The undercooling under higher PO_2 than the ones evaluated in experiment 2 can be verified using Ar provided the PO_2 remains below approximately 10^{-18} atm. This is the value of oxygen in equilibrium with Ti/TiO_2 at 1400 °C (this is the temperature of the Ti sponge inside the main furnace, as shown in Figure 2). If the gas coming in the furnace has a PO_2 below 10^{-18} atm, the Ti-sponge basket does not have a major effect on the gas composition and the oxygen partial pressure measured at the exit is representative of the oxygen in equilibrium with the metal sample. If the incoming gas has a PO_2 higher than 10^{-18} atm, then the Ti will react with the oxygen and the PO_2 measured downstream is meaningless (around 10^{-18} atm while there is sufficient Ti). This was verified by using two oxygen sensors, one in the entrance and another at the exit.

The effect discussed previously can be observed in experiment 3. In this case, nine cooling experiments were performed in a row. The first experiments were done with Ar/H_2 but with Ti that has been already used inside the furnace; under these conditions, the initial PO_2 was higher than the initial value measured in experiment 2. After the fourth undercooling (experiment 3D), the gas was switched to Ar and the PO_2 experienced an increase to 10^{-18} atm and above. Figure 5 shows the change in undercooling in experiment 3 and Figure 6 the change in contact angle.

Experiments 3A through 3D show that the high undercooling achieved with Ar in experiment 2H can also be achieved with Ar/H_2 if the PO_2 is not very low. The most important change was observed from experiments 3E through 3F. The sample was observed to change from not wetting (contact angle 91.5 deg) to wetting (contact angle 75.5 deg). The change in the wetting behavior was followed by a sudden drop in undercooling from 273 °C to 118 °C. This simultaneous change in wetting behavior and undercooling was verified with additional experiments.

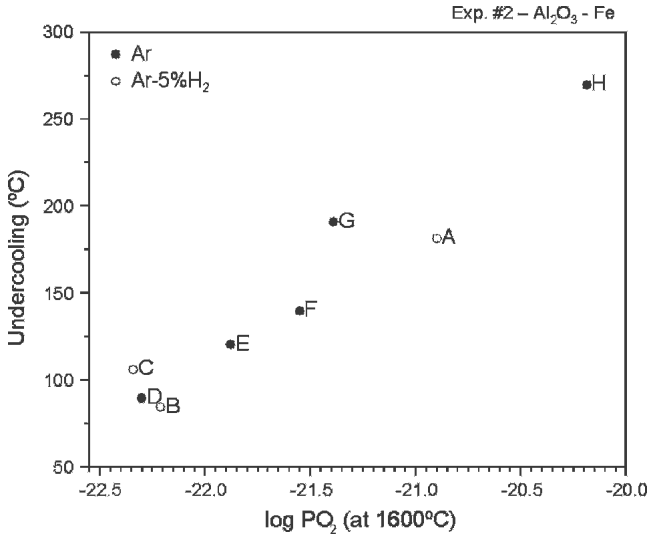

Fig. 4—Change in undercooling during experiment 2. The letter next to each point refers to the order in the sequence of multirecalescense experiments—the PO_2 is the average for the hour that the sample remains at 1600 °C before cooling.

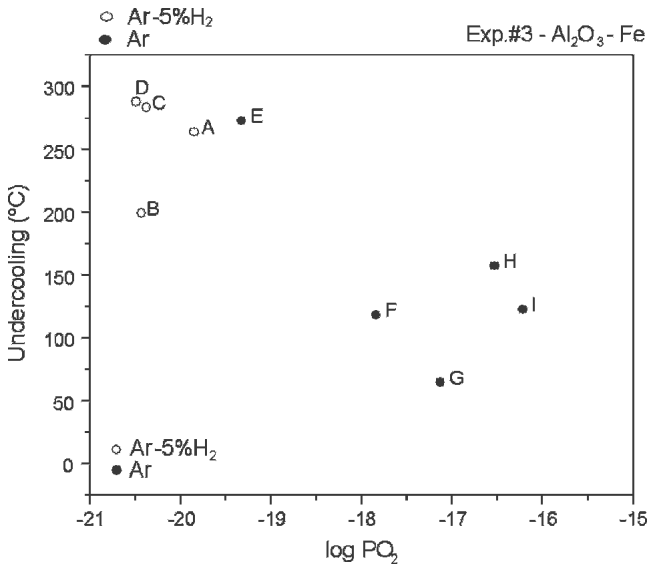

Fig. 5—Change in undercooling during experiment 3. The letter next to each point refers to the order in the sequence of multirecalescense experiments—the PO_2 is the average for the hour that the sample remains at 1600 °C before cooling.

In experiment 3 with PO_2 above 10^{-18} atm, the real oxygen ''seen'' by the sample is higher than the value measured downstream and it is therefore unknown. This is evident through a change in contact angle (Figure 7) unexpected for the measured PO_2. However, the results are useful because they show that the undercooling also decreases with increasing oxygen content.[42] In order to have an accurate estimation of the effect of increasing oxygen content in undercooling; the intermediate range of PO_2 was covered by using $CO\text{-}CO_2$ mixtures instead of Ar, and the higher range of PO_2 was covered with nongettered Ar.

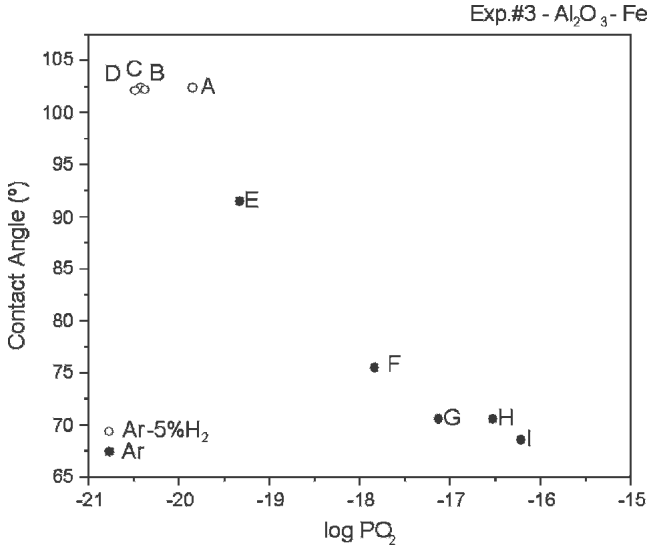

Fig. 6—Change in contact angle with oxygen partial pressure for experiment 3. The letter next to each point refers to the order in the sequence of multirecalescense experiments—the PO_2 is the average for the hour that the sample remains at 1600 °C before cooling.

The average results after more than 130 undercooling experiments for the Fe/Al_2O_3 system are shown in Figure 8 and the contact angle in Figure 9. No distinction was made between single crystals and polycrystalline substrates, since no difference was observed in the results.

The experimental results indicated that the contact angle for Fe/Al_2O_3 goes through a maximum of 130 deg for an oxygen partial pressure between 10^{-20} and 10^{-19} atm. The contact angle decreases to values as low as 95 deg for $PO_2 = 10^{-22}$. The mechanism that makes the liquid metal wet the solid substrate at low PO_2 also promotes a lower undercooling. On the other hand, in the range of intermediate PO_2, in which nonwetting behavior is observed, the undercoolings are as high as 290 °C. The maximum undercooling achieved under these conditions is close to the hypercooling limit[9] for iron and also to some values reported as representative of homogeneous nucleation undercooling[11] (Turnbull, Table I). As the oxygen partial pressure increased, the undercooling was observed to decrease to an average of slightly higher than 100 °C. The change in undercooling was accompanied also by a drop in the contact angle and in some cases by the formation of hercynite ($FeAl_2O_4$).

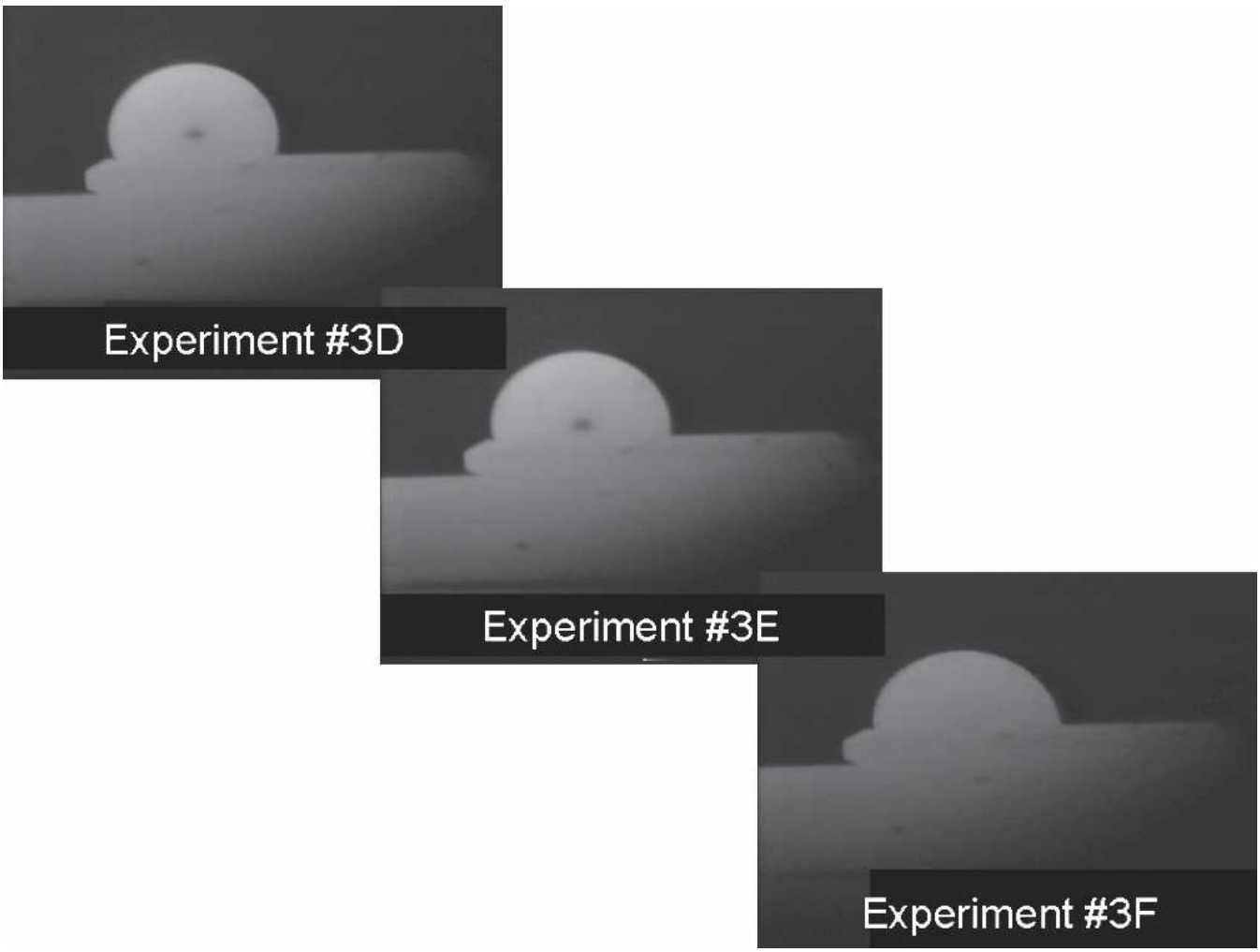

Fig. 7—Change in contact angle from experiment 3D to 3F.

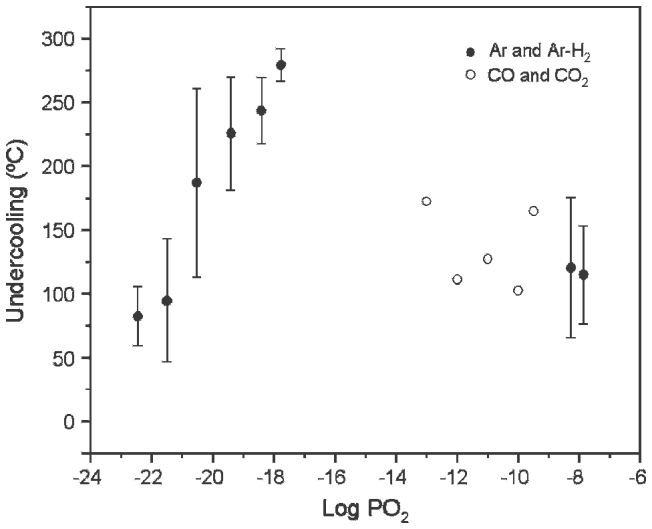

Fig. 8—Average undercooling as a function of PO_2 for Fe/Al_2O_3.

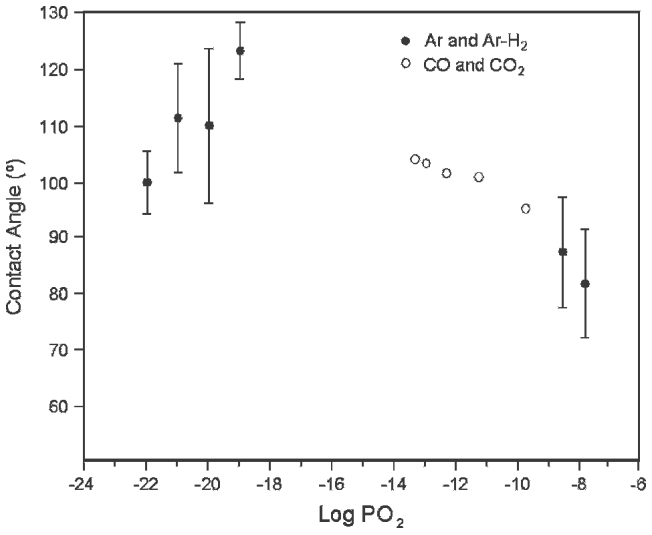

Fig. 9—Average contact angle as a function of PO_2 for Fe/Al_2O_3.

B. *Undercooling Measurement in the DTA*

The behavior discussed for the sessile drop experiments was verified in the DTA by running consecutive experiments using the same pure iron sample on Al_2O_3 crucibles (Figure 10).

In the DTA, the undercooling decreases to almost 0 °C for very low oxygen partial pressures, increases to undercooling above 250 °C for intermediate PO_2, and then drops to below 50 °C with a further increase in oxygen. The arrow in the bottom-right experimental point in Figure 10 has the same meaning discussed for the sessile drop experiments: the real PO_2 in this point may be higher. Another important point to highlight is that deep undercoolings were measured for both Ar and Ar-H_2 experiments. The horizontal dotted line on Figure 10 corresponds to the results by Mizoguchi.[15] In his article, an undercooling of 164 °C for pure iron on the Al_2O_3 crucible was the maximum value

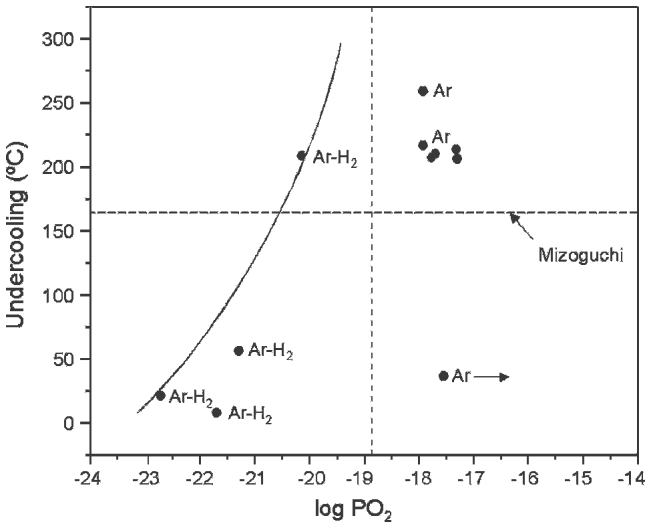

Fig. 10—Undercooling measurement on DTA for pure iron on Al_2O_3 crucibles.

achieved when no particles were added to the metal (Table I); the gas used was ultra-high-purity Ar, but no oxygen partial pressure was reported.

C. *Analysis of the Samples after the Experiments*

The SEM analysis of the samples after the experiments gave information on the interaction between the substrate and the liquid metal. The cross-sectional analysis of the Fe/Al_2O_3 system showed that after Ar/H_2 experiments or experiments under Ar with low oxygen partial pressure, there was no reaction layer between the droplet and the substrate, while in the case of the experiments under high oxygen partial pressures (nongettered Ar, for example), there was a layer with Fe, Al, and O (the stoichiometric analysis suggests it is hercynite). The experiments under CO/CO_2 showed no hercynite in the interface. In the case of sequenced experiments that were first subjected to a PO_2 that should produce hercynite, and then to low PO_2, a composed interface of Fe and Al_2O_3 was observed, confirming the decomposition of the previously formed hercynite.

Alumina particles were found on the surface of droplets that were melted and solidified under Ar-H_2 (or low PO_2). The sample was originally pure iron so the inclusions should have been caused by dissolution of the substrate and reprecipitation. The results from the substrate analysis are summarized in Figure 11.

V. DISCUSSION

A. *Relation between Undercooling and Wettability*

The focus of this work is on the effect of the oxide-metal interface as a heterogeneous nucleation site. The change in contact angle for Fe/Al_2O_3 confirmed a behavior already reported. The contact angle goes through a maximum of 130 deg for an oxygen partial pressure between 10^{-20} and $10^{-18.5}$ atm. The mechanism that made the liquid metal wet the oxide at high and low PO_2 also promoted a lower undercooling (below 100 °C). The maximum undercooling

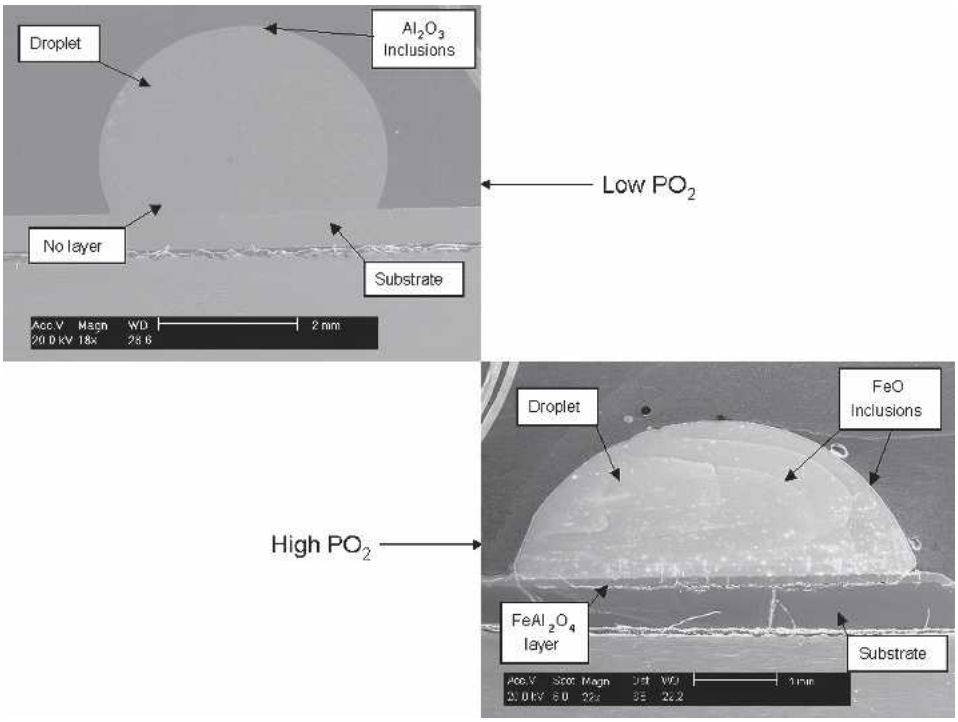

Fig. 11—Cross section of a nonwetting droplet after a low PO_2 (below range covered by CO-CO_2) experiment and a wetting droplet after a high PO_2 ($>10^{-8}$ atm) experiment.

achieved under these conditions was close to the undercooling reported by Turnbull for homogeneous nucleation of Fe droplets. The presence of a maximum in undercooling was verified in the DTA experiments using Al_2O_3 crucibles.

The presence of Al_2O_3 inclusions in the material shows that the substrate decomposed to achieve equilibrium with the metal and the oxygen in the gas. Several authors[36,40] have reported the presence of Al and Zr dissolved in iron droplets that were placed in contact with Al_2O_3 and ZrO_2 crucibles or substrates. This suggests that the change in PO_2 not only produces a change in the oxygen dissolved in the droplet but also on the aluminum content.

The system (droplet/substrate) reacts to changes in the gas composition by changing its contact angle and the temperature in which heterogeneous nucleation on the substrate occurs. These two values (contact angle and undercooling) are not directly related because they describe different phenomena, but there are common variables that affect both. Figure 12 shows that the contact angle θ is a function of γ_{LG}, γ_{OL}, and γ_{OG} while the heterogeneous nucleation undercooling is a function of the contact angle θ' that is in fact a function of γ_{LS}, γ_{OS}, and γ_{OL}. The common surface to both undercooling and wettability is the oxide-liquid interface (*OL*).

Considering γ_{OG} constant and the γ_{LG} changing with the Jimbo and Cramb equation,[43] the maximum in contact angle (θ) requires a maximum in the value of γ_{OL} with oxygen partial pressure. The drop in γ_{OL} may be caused by the dissolution of the substrate in the low range of PO_2 and by the oxygen for high PO_2. However, a decrease in the surface energy of the oxide-liquid interface would not explain the drop in undercooling under the assumption that

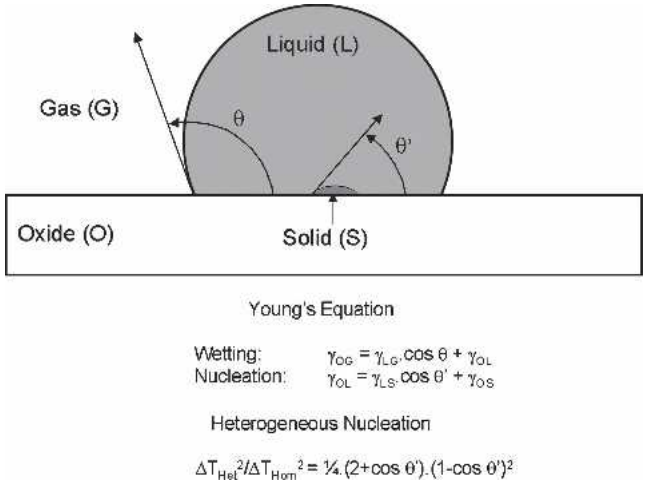

Fig. 12—Schematic and Young's equations for the contact angle for wetting (θ) and contact angle for heterogeneous nucleation (θ').

nucleation occurs according to the classical theory (providing γ_{OS} and γ_{LS} remain constant). Under the classical nucleation theory, a decrease in γ_{OL} implies an increase in the heterogeneous nucleation undercooling. On the other hand, the change in γ_{OL} can be analyzed from the point of view of the degree of interaction between the liquid and the oxide. Figure 13 shows the calculated change in work of adhesion (*Wa*) and γ_{OL} for Fe/Al_2O_3 as a function of contact angle; the calculation was made using the published values of surface tension (γ_{LG} = 1891.3 mN/m[43], γ_{OL} = 1700 mN/m,[44] and γ_{OG} = 650 mN/m[44]). The degree of

interaction between the liquid and the oxide increases as the contact angle decreases. If the contact angle is 180 deg, there is no interaction between the liquid and the oxide, the work of adhesion is zero, and the γ_{OL} is a maximum. As the contact angle decreases, the work of adhesion increases as does the interaction between liquid and metal and the γ_{OL} decreases.

The results of this analysis suggest that as the γ_{OL} increases, and the interaction between liquid and oxide decreases, the undercooling should increase from heterogeneous to homogeneous nucleation. An alternative explanation that is useful to relate the changes in contact angle and undercooling is that the increase in wettability implies an increase in the area wetted by the metal, and hence an increase in the effective surface where heterogeneous nucleation can occur.

This analysis (Figure 13) also implies that as the wettability decreases, the undercooling approaches the expected value for homogeneous nucleation. This is the case for the experiments presented in this work: the value of undercooling under a condition where a heterogeneous nucleation surface was clearly available was similar to the maximum undercooling reported by Turnbull[11] for homogeneous nucleation (295 °C).

B. *Effect of Dissolution of Substrate*

Some authors[12,13,45–47] have reported a maximum in contact angle of Ni/Al_2O_3 and Fe/Al_2O_3 with oxygen. They had attributed the decrease of contact angle to lower oxygen partial pressures, to the increase in the aluminum dissolved in the metal. Since, in equilibrium with Al_2O_3, the lower the oxygen content, the higher the dissolved aluminum content, this effect could explain the drop in contact angle as the PO_2 decreases. Then, if the decrease in undercooling observed in the experiments with low PO_2 is caused by the increase in the elements introduced in the metal during the substrate dissolution, the undercooling on experiments using steels with high aluminum should show low values of undercooling, as observed by Kudoh.[13]

The same sessile drop experimental setup (under Ar-H_2–PO_2:10^{-22} to 10^{-21}) and the DTA (under gettered Ar) were used to evaluate the undercooling of steel samples with Al contents ranging from 0.009 to 1.224 pct Al.[48] The preliminary results in the sessile drop furnace showed that the undercooling increased in each cycle; this increase may be caused by the aluminum leaving the sample. The decrease in Al content in the sample can be estimated by looking at the variation in melting temperature during heating in the DTA experiments. Figure 14 shows the undercooling as a function of melting temperature.

It is clear from this graph that the sample is becoming purer. This becomes evident through the increase in the melting temperature. As the sample loses aluminum, the undercooling increases. In Figure 14, the range of maximum undercooling measured for the pure iron experiments on Al_2O_3 in the sessile drop experiments is also shown. These are the points in which the sample is purest, low oxygen due to low PO_2 and low Al due to limited dissolution of the substrate. These results agree with the hypothesis that the decrease in undercooling in the low PO_2 range is caused by the introduction of Al from the dissolution of the substrate.

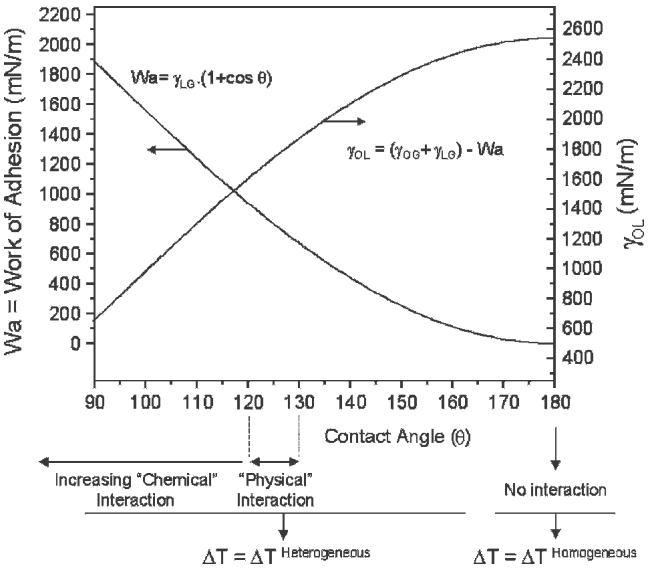

Fig. 13—Calculated change in work of adhesion (*Wa*) and γ_{OL} for Fe/Al_2O_3.

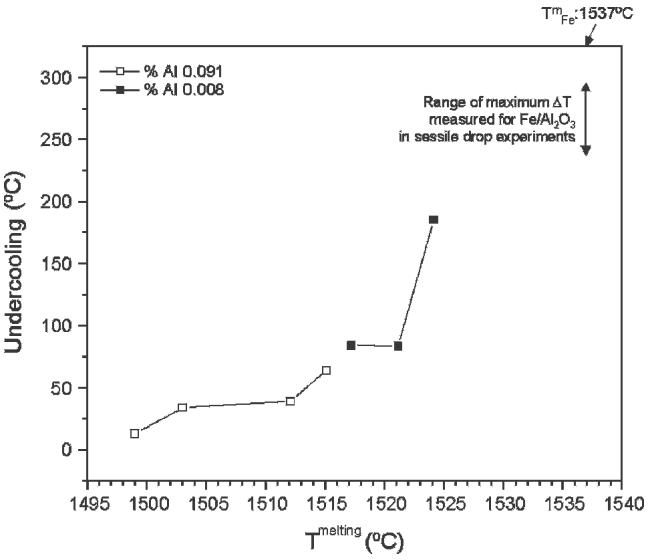

Fig. 14—Increase of undercooling with increasing melting temperature (decreasing aluminum) measured by DTA.

It is clear from our experiments that a parameter that is a function of the two solid lattices is not sufficient to define the undercooling. This is due to the observed effect of the metal composition (oxygen and aluminum) on the undercooling. The degree of misfit between the solid (S) and the nucleant (O) can be described with Bramfitt's planar lattice disregistry.[49] Bramfitt used this parameter to explain the difference in efficiency as the heterogeneous nucleant of delta ferrite, exhibited by different carbides and nitrides, by measuring the degree of undercooling during solidification. Many researchers have referred to this parameter.[16,50,51] Grong[52] collected values of undercooling of steel with different types of inclusions and concluded that the undercooling was proportional to the square root of Bramfitt's planar lattice disregistry. According to his work,

the undercooling necessary for nucleation of δ-iron (111) on Al_2O_3 (0001) is a little bit greater than 10 °C. Our experiments indicate that the undercooling of Fe on Al_2O_3 could vary from 0 °C to 290 °C and indicate that a lattice disregistry approach to prediction of heterogeneous nucleation, while it may be predictive of trends, is not a complete methodology in the prediction of nucleation effects in alloys.

C. *Solidification Rate*

The direct observation of the solidification of the sessile droplets allows for the verification that solidification starts on the substrate and also for the observation of the movement of the solidification front. This is clearer in those experiments that show relatively low undercoolings, where the solidification front moves across the sample from bottom (substrate) to top at a slower rate. The solidification starts right after a ''bright flash,'' as shown in Figure 1, and the sample remains bright during solidification. For deep undercoolings, the droplet solidifies in fractions of a second and the error in the estimated rate increases due to the limit imposed by the acquisition rate of the camera (30 frames/s). On the other hand, if the undercooling is very low, the recalescense it is almost zero and only the total solidification time can be estimated from the change in the shape of the droplet. The solidification rate was measured as the change in position of the interface with time (*dm*/*dt*). As an example, Figure 15 shows the curves for three undercooling experiments at 71 °C, 104 °C, and 283.5 °C. The modeling of the growth rate has been published previously.[53]

The average solidification rate is the droplet size divided by the total solidification time. As expected, the solidification rate depends on the degree of undercooling (Figure 16).

It can be seen from the figure that the average solidification rate can be as high as 9 mm/s. This is a very high solidification rate considering that is not an initial and instantaneous rate but the average solidification rate of a droplet of approximately 3-mm height. Because recalescense causes the liquid to lose its initial undercooling, the assumption of constant undercooling is meaningful only in the start of solidification. The decrease in solidification rate after the onset of solidification depends on the heat transfer out of the interface.[53] Regardless of the actual average undercooling, it is a fact that the solidification rate is faster in an undercooled liquid than under conditions found when using a water-cooled copper mold.[54]

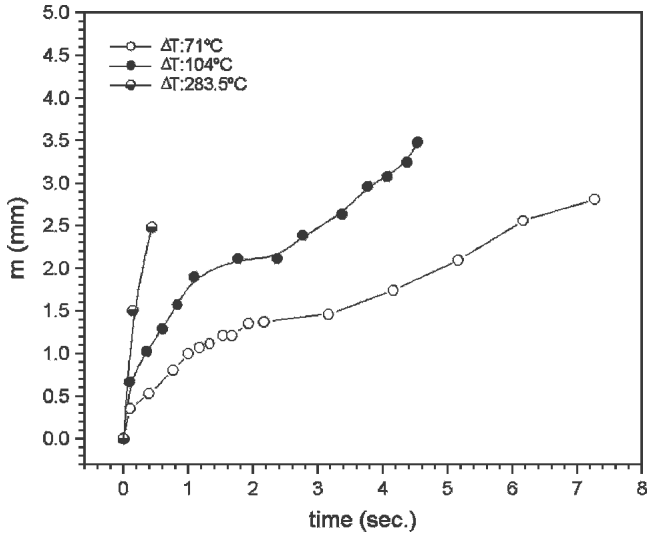

Fig. 15—Change in the position of the solidification front.

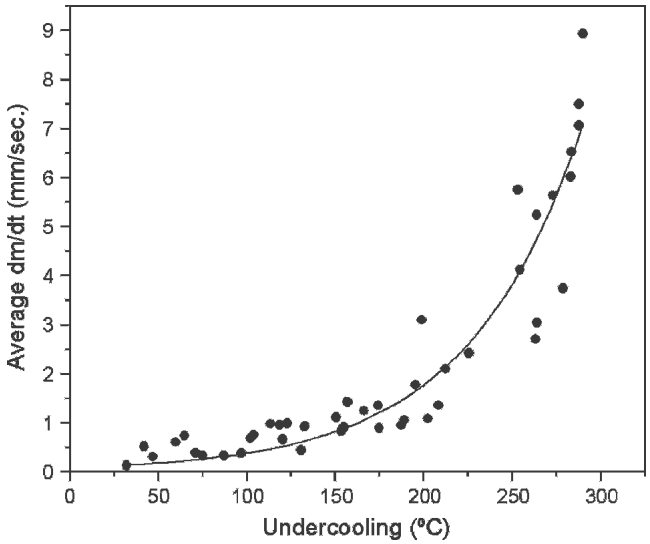

Fig. 16—Average solidification rate as a function of undercooling for pure iron.

VI. CONCLUSIONS

The main conclusion of this work is that the undercooling of liquid iron, when an Al_2O_3 surface is present, is not only a property of the metal/oxide couple but is also dependent on the oxygen partial pressure. The experimental results indicated that the undercooling of liquid iron, in contact with an Al_2O_3 substrate, did not have a unique value, varied from 0 °C to 290 °C, and was significantly affected by the oxygen content of the gas phase and the degree of interaction between the oxide and the metal. Deep undercoolings are possible at low oxygen potentials, provided the oxygen potential is such that substantial substrate decomposition does not occur. The measured undercooling was a strong function of gas phase oxygen content, and a maximum in undercooling of 290 °C was measured at $PO_2 = 10^{-19}$. The variation in undercooling was related to the wetting of the substrate by the liquid metal, where the deepest undercoolings occurred when the highest contact angle between the substrate and the liquid droplet was achieved.

Thus, it is not sufficient to establish the inclusion composition to define an undercooling, as changes in the steel composition (for example, oxygen content or aluminum) can lead to conditions that vary from low to high undercoolings. This is probably due to variations in interfacial composition at the liquid iron–alumina interface and indicates that the potential for a surface to be a nucleating agent is a function not only of the surface but also of the details of the composition of the liquid in contact with the surface and that, at least in the case of alumina, slight modification

in elements that segregate to surfaces can markedly affect the ability of a surface to be a heterogeneous nucleant. This may explain the variations observed in the solidification structure during the normal casting practice.

ACKNOWLEDGMENTS

The authors thank the member companies of the Center for Iron and Steelmaking Research, Carnegie Mellon University, and the AISI DOE Project 0101—"Inclusion Optimization for New Generation Steel Products"—for the financial support.

REFERENCES

1. J. Takamura and S. Mizoguchi: *Proc. 6th Int. Iron Steel Congr.*, Nagoya, 1990, pp. 21–26 and 591-604.
2. A.O. Kluken and O. Grong: *Metall. Trans. A*, 1989, vol. 20A, p. 1335-49.
3. C.E. Cross, O. Grong, and M. Mousavi: *Scripta Mater.*, 1999, vol. 40 (10), pp. 1139-44.
4. A.O. Kluken, O. Grong, and G. Rorvik: *Metall. Trans. A*, 1990, vol. 21A, p. 2047.
5. J. Kim: Master's Thesis, Carnegie Mellon University, Pittsburgh, PA, 2005.
6. H. Fujimura, S. Tsuege, Y. Komizo, and T. Nishizawa: *Tetsu-to-Hagané*, 2001, vol. 87 (11), pp. 29-34.
7. T.E. Quested: *Mater. Sci. Technol.*, 2004, vol. 20, pp. 1357-69.
8. A.L. Greer, P.S. Cooper, M.W. Meredith, W. Schneider, P. Schumacher, J.A. Spittle, and A. Tronche: *Adv. Eng. Mater.*, 2003, vol. 5 (1–2), pp. 81-91.
9. M. Flemings and Y. Shiohara: *Mater. Sci. Eng.*, 1984, vol. 65, pp. 157-70.
10. T.Z. Kattamis and M.C. Flemings: *Trans. AIME*, 1966, vol. 236, pp. 1523-32.
11. D. Turnbull and R.E. Cech: *J. Appl. Phys.*, 1950, vol. 21, pp. 804-10.
12. Y. Gao, M. Kudoh, and K. Ohsasa: *Bull. Faculty Eng., Hokkaido Univ.*, 1990, vol. 149, pp. 49-59.
13. M. Kudoh, K. Ohsasa, K. Tanaka, and K. Okuyama: *Bull. Faculty Eng., Hokkaido Univ.*, 1992, vol. 162, pp. 191-202.
14. R. Rastogi: Ph.D. Thesis, Carnegie Mellon University, Pittsburgh, PA, 2000.
15. K. Nakajima, H. Hasegawa, S. Khumkoa, and S. Mizoguchi: *Metall. Mater. Trans. B*, 2003, vol. 34B, pp. 539-47.
16. A. Abedi, M. Kudoh, and Y. Itoh: *Iron Steel Inst. Jpn. Int.*, 1997, vol. 37 (8), pp. 770-75.
17. G. Abbaschian and M.C. Flemings: *Metall. Trans. A*, 1983, vol. 14A, pp. 1147-57.
18. T. Koseki and M.C. Flemings: *Metall. Trans. A*, 1995, vol. 26A, pp. 2991-99.
19. Y. Shiohara, M.C. Flemings, Y. Wu, and T.J. Piccone: *Trans. Iron Steel Inst. Jpn.*, 1986, vol. 26, pp. B131-B134.
20. T.J. Piccone, Y. Wu, Y. Shiohara, and M.C. Flemings: *Metall. Trans. A*, 1987, vol. 18A, pp. 925-32.
21. Y. Guan, B. Song, and J. Mao: *Acta Metall. Sinica*, 2003, vol. 39 (3), pp. 283-86.
22. K. Nakajima, H. Hasegawa, S. Khumkoa, and S. Mizoguchi: *Metall. Mater. Trans. B*, 2003, vol. 34B, pp. 539B-547B.
23. N. Eustathopoulos, M.G. Nicholas, and B. Drevet: *Wettability at High Temperatures*, Pergamon, Amsterdam, NY, 1999.
24. S. Ueda, H. Shi, X. Jiang, H. Shibata, and A.W. Cramb: *Metall. Mater. Trans. B*, 2003, vol. 34B, pp. 503-08.
25. K. Ogino, K. Nogi, and Y. Koshida: *Tetsu-to-Hagané*, 1973, vol. 59 (10), pp. 1380-87.
26. K. Ogino, A. Adachi, and K. Nogi: *Tetsu-to-Hagané*, 1973, vol. 59 (9), pp. 1237-44.
27. N. Takiuchi, T. Taniguchi, N. Shinozaki, and K. Mukai: *J. Jpn. Inst. Met.*, 1991, vol. 55 (1), pp. 44-49.
28. Z. Jun and K. Mukai: *Iron Steel Inst. Jpn. Int.*, 1998, vol. 38 (10), pp. 1039-44.
29. B.T. Eldred and P.D. Ownby: *Trans. JWRI*, 2001, vol. 30, pp. 69-74.
30. N. Shinozaki, T. Fujita, and K. Mukai: *Metall. Mater. Trans. B*, 2002, vol. 33B, pp. 506-09.
31. Z. Yuan, K. Mukai, K. Takagi, and M. Ohtaka: *J. Jpn. Inst. Met.*, 2001, vol. 65 (1), pp. 21-28.
32. A.T. Hasouna, K. Nogi, and K. Ogino: *Trans. Jpn. Inst. Met.*, 1998, vol. 29 (9), pp. 748-55.
33. D.R. Gaskell: *Introduction to the Thermodynamics of Materials*, 3rd ed., Taylor and Francis, Washington, D.C., 1995.
34. R. Fruehan: *The Shaping and Treating of Steel*, 11th ed., The AISE Steel Foundation, Pittsburgh, PA, 1998.
35. B. Gallois and C.H.P. Lupis: *Metall. Trans. B*, 1981, vol. 12B, pp. 549-57.
36. K. Nakashima, K. Takihira, K. Mori, and N. Shinozaki: *Mater. Trans., JIM*, 1992, vol. 33 (10), pp. 918-26.
37. H. Shibata, X. Juang, M. Valdez, and A. Cramb: *Metall. Trans. B*, 2004, vol. 35B, pp. 179-81.
38. Z. Jun and K. Mukai: *Iron Steel Inst. Jpn. Int.*, 1998, vol. 38 (10), pp. 1039-44.
39. P. Shen, H. Fujii, T. Matsumoto, and K. Nogi: *Acta Mater.*, 2003, vol. 51, pp. 4897-906.
40. K. Nakashima, K. Takihira, T. Miyazaki, and K. Mori: *J. Am. Ceram. Soc.*, 1993, vol. 76 (12), pp. 3000-08.
41. H. Biloni and W. Boettinger: *Physical Metallurgy*, 4th ed., Elsevier Science, New York, NY, 1996, ch. 8.
42. A. Abedi, M. Kudoh, and Y. Itoh: *Iron Steel Inst. Jpn. Int.*, 1995, vol. 52 (6), pp. 589-95.
43. A.W. Cramb and I. Jimbo: *Steel Res.*, 1989, vol. 60, pp. 157-65.
44. *Slag Atlas*, 2nd ed., Verlag Stahleisen GmbH, Düsseldorf, Germany, 1995.
45. B.L. Jones and G.M. Weston: *J. Austr. Inst. Met.*, 1970, vol. 15 (4), pp. 189-94.
46. C. Wan, P. Krisalis, B. Drevet, and N. Eustathopoulos: *Mater. Sci. Eng., A*, 1996, vol. 207, pp. 181-87.
47. V. Merlin and N. Eustathopoulos: *J. Mater. Sci.*, 1995, vol. 30, pp. 3619-24.
48. K. Fuchigami: Master's Thesis, Carnegie Mellon University, Pittsburgh, PA, 2005.
49. B.L. Bramfitt: *Metall. Trans.*, 1970, vol. 1.
50. G.N. Heintze and R. McPherson: *Welding Res. Suppl.*, 1986, pp. 71s-82s.
51. A. Ostrowski and E.W. Langer: *Scand. J. Metall.*, 1979, vol. 8, pp. 177-84.
52. O. Grong: *Metallurgical Modeling of Welding*, 2nd ed., The Institute of Materials, London, 1997.
53. M. Valdez, H. Shibata, S. Sridhar, and A.W. Cramb: *Materials Science and Technology Conf.*, New Orleans, LA, 2004.
54. N. Phinichka: Ph.D. Thesis, Carnegie Mellon University, Pittsburgh, PA, 2001.